

Electron-impact single ionization of multiply charged manganese ions

R. Rejoub and R. A. Phaneuf

Department of Physics, University of Nevada, Reno, Nevada 89557-0058

(Received 27 September 1999; published 10 February 2000)

Absolute cross sections have been measured for single ionization of Mn^{q+} ($5 \leq q \leq 8$) by electron impact at energies ranging from the ionization thresholds to 4 keV using a new dynamic-crossed-beams apparatus. The experimental cross sections are essentially featureless, but show evidence for significant contributions due to $3p \rightarrow nl$ ($n \geq 4$) inner-shell excitation followed by autoionization for Mn^{5+} and Mn^{6+} , and $3s \rightarrow nl$ ($n \geq 5$) excitation-autoionization for Mn^{7+} and Mn^{8+} . The measurements for Mn^{6+} and Mn^{8+} and their interpretation are complicated by the presence of an undetermined fraction of the primary ion beams in metastable states.

PACS number(s): 34.80.Kw

I. INTRODUCTION

Qualitative and quantitative knowledge of the physics of charge-changing collisions is fundamental to understanding the behavior of a wide variety of naturally occurring and man-made plasmas [1]. In particular, the modeling of non-equilibrium plasmas requires accurate cross sections for excitation, ionization, and recombination of ions by electron impact. Metallic ions of elements in the fourth row of the Periodic Table are of particular importance in both astrophysical and fusion plasmas because of their nuclear stability and mechanical properties. Their electronic structure when partially ionized is sufficiently complex to render semiempirical scalings such as the Lotz formula [2] unreliable for predicting cross sections for ionization by electron impact [3,4]. Laboratory cross-section measurements have been reported for ionization of multiply charged ions of Sc [5], Ti [6–11], Cr [12], Fe [8,13–16], Ni [17–19], and Cu [17]. These data indicate contributions to the total ionization cross sections due to inner-shell excitation followed by autoionization that range from insignificant to dominant, depending on the initial charge and electronic structure of the ion. Theoretical calculations based on the distorted-wave approximation that include this indirect ionization mechanism [20–22] have been relatively successful in accounting for the magnitudes of the measured total single ionization cross sections for multiply charged metallic ions.

This paper reports absolute cross-section measurements made using a new dynamic-crossed-beams apparatus developed to investigate the various mechanisms contributing to the electron-impact ionization of multicharged ions. The measurements for Mn^{q+} ions ($5 \leq q \leq 8$) are believed to be the first for ions of this element, and were conducted in order to investigate systematic effects in the ionization of multiply charged metallic members of the Cl, Ar, K, and Ca isoelectronic sequences. This work represents the initial stage of a program to conduct parallel investigations of ionization of multiply charged ions by electron and photon impact.

II. EXPERIMENT

A. Dynamic-crossed-beams method

The principle of the dynamic-crossed-beams method [23,24] is to intersect a well-collimated beam of positive ions

of known energy and charge state with an electron beam of variable energy at right angles, and to sweep the electron beam completely across the ion beam in a linear motion at constant speed. The absolute ionization cross section σ in cm^2 for a given electron-impact energy is determined from the following expression, in which all the required parameters are measured experimentally:

$$\sigma = K \frac{v_e v_i q e^2 u}{I_e I_i (v_e^2 + v_i^2)^{1/2}}. \quad (1)$$

K is the total number of further ionized product ions accumulated during one sweep of the electron beam across the ion beam, v_e and v_i are the electron and ion velocities in cm/sec , q is the charge state of the ion, e is the electronic charge in Coulombs, u is the sweep speed of the moving electron beam in cm/sec , and I_e and I_i are the total electron and ion beam currents in amperes. The background of product ions produced by stripping collisions of the ion beam with residual gas is determined by the counts produced in the detector when the electron beam is near the extreme positions of its linear travel, where the beams do not intersect.

The layout of the dynamic-crossed-beams apparatus developed for ionization cross-section measurements based on this method is presented in Fig. 1.

B. Ion beam

The experiments were performed at the Multicharged Ion Research Facility at the University of Nevada, Reno [25]. Multiply charged ^{55}Mn ions were produced in a 14.4 GHz Caprice electron-cyclotron-resonance (ECR) ion source [26]. Manganese metal was introduced into the ECR ion source using an axially inserted tungsten micro-oven which replaced the normal first-stage plasma tube. Ions were extracted from the source discharge through a potential difference of 10 kV, electrostatically focused and momentum-per-charge selected using a double-focusing magnetic spectrometer. The ion beamline transport system consisted of three einzel lenses, two sets of electrostatic horizontal and vertical steering plates, and three stages of differential pumping. The vacuum in the ion beamline just upstream of the crossed-beam apparatus was typically 1×10^{-9} torr under operating conditions.

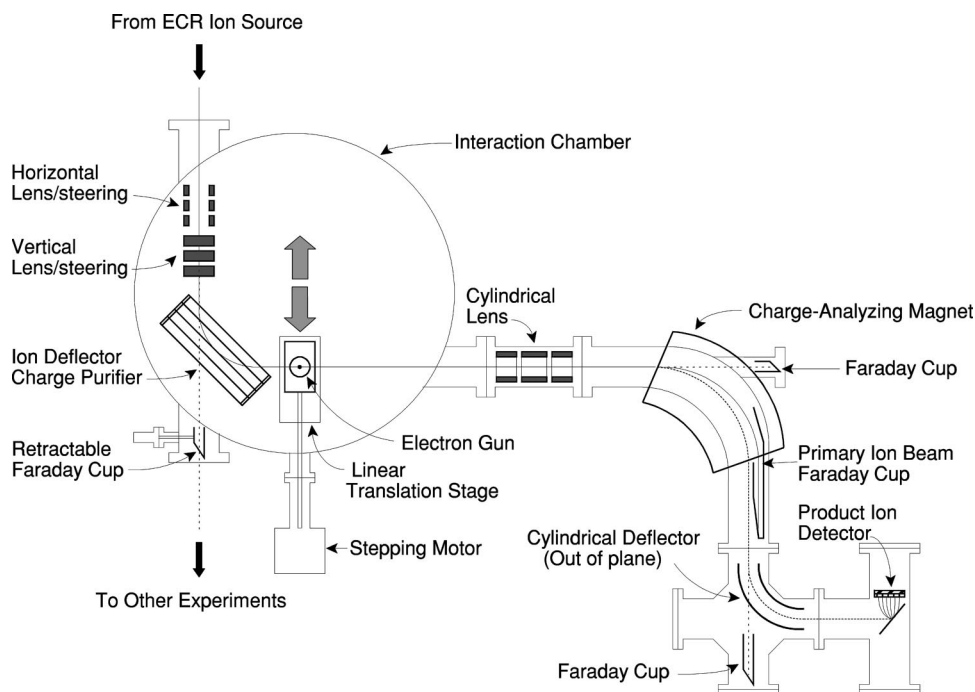


FIG. 1. Schematic of dynamic-crossed-beams apparatus for absolute measurements of electron-impact ionization of multiply charged ions.

The operating Mn^{q+} ion beam currents in the experiment ranged from 30 nA to 800 nA, with an approximately 2 mm diameter at the point of intersection with the electron beam.

C. Electron beam

The electron beam was produced by a high-energy electron gun [27] developed and fabricated at Justus-Liebig University in Giessen, Germany. The electron gun was mounted on a ball-slide linear translation stage such that the electron beam axis was vertical. The gun assembly could be translated horizontally back and forth across the ion beam axis via a computer-controlled stepping motor connected to a precision linear-motion feedthrough. The electron beam itself was produced by an indirectly heated tungsten dispenser cathode, focused electrostatically to a diameter of 1–2 mm, passed through a field-free region where it intersected the ion beam, then defocused and collected in a water-cooled anode. Typical electron beam currents were 1 mA at 100 eV and 50 mA at 4 keV. The energy of the electron beam was determined to an accuracy of better than 1% by measuring the voltage applied to the cathode using a voltage divider calibrated and read by a precision digital voltmeter. A 2 eV correction to the beam energy due to the contact potential of the cathode was determined by measurement of the known $1s \rightarrow 2s$ excitation-autoionization step in electron-impact ionization of O^{5+} at 550 eV [28]. From this measurement, the energy spread in the electron beam was determined to be 2.4 eV (full width at half maximum). This value is consistent with the measurement of Stenke *et al.* for an identical electron gun [27], and suggests that at the operating pressure of 5×10^{-9} torr, the space charge in the electron beam was being neutralized to a significant extent by trapped ions produced from the residual gas. This condition has been shown to be important for avoiding spurious signals attributed to space-charge interaction of the electron and ion beams [29].

D. Cross-section measurement

The ion beam of selected mass and charge state was directed into the crossed-beams interaction chamber, where one-dimensional einzel lenses provided independent vertical and horizontal focusing and positioning of the ion beam. A parallel-plate analyzer directed the ion beam to the interaction region where the electron gun is located, and served to remove ions from the beam that had changed charge during transport from the selector magnet (a path of approximately 2.5 m). After passing the interaction region, the ion beam (which also contained further ionized product ions) was focused by a cylindrical einzel lens. The product ions were separated from the primary beam by a dipole charge-analyzing magnet, such that the product ions were deflected through 90° . The primary ions were deflected through a smaller angle (depending on the final-to-initial charge ratio) and collected by an extended Faraday cup mounted inside the magnet chamber. The product ions were further deflected by a 90° cylindrical electrostatic analyzer out of the plane in which the primary beam was analyzed and collected. In order to ensure a product ion detection efficiency near unity, a special product ion detector was developed based on the principle that the incident ions each produce a number of secondary electrons when incident upon an inclined metal surface (converter plate) [30]. These electrons were accelerated through 450 V to a microchannel plate detector, which provided the charge pulses to be counted.

An important criterion for the determination of an absolute cross section is the complete transmission of product ions to their detector. This condition was assured by first transporting the primary ion beam to the Faraday cup located behind the final cylindrical deflector for the product ions (with its electrodes grounded), and then scaling the charge-analyzer magnetic field and downstream cylindrical lens by

TABLE I. Experimental uncertainties in absolute ionization cross-section measurements estimated at 90% confidence level.

Source of uncertainty	Percent uncertainty
Counting statistics ^a (2 standard deviations of the mean)	± 2%
Background subtraction ^a	± 3%
Signal ion detection and pulse transmission	± 5%
Ion transmission to Faraday cup	± 3%
Ion current measurement	± 2%
Electron current measurement	± 2%
Electron gun translation speed	± 2%
Quadrature sum	± 8%

^aEstimated at electron energies near the cross-section maximum.

the appropriate charge ratio to direct the product ions onto their detector. This scaling simultaneously placed the primary ion beam in the main Faraday cup. The criterion adopted for ion beam transmission was that the currents measured in these two Faraday cups (appropriately biased to suppress secondary electron emission) did not differ by more than a few percent. Satisfying this condition required careful tuning of the ion beam, and the percent difference between these two current measurements was used as a contributing uncertainty to the absolute cross section. By monitoring the product ion count rate, small adjustments could then be made to the analyzing magnetic field and cylindrical deflector to center the product ion beam on the detector. Such measurements verified that the product ion beam diameter was several times smaller than that of the detector. As an initial test of the new apparatus, absolute cross-section measurements were made for electron-impact single ionization of Ar^{6+} from 100 eV to 2500 eV, and compared to absolute crossed-beam measurements reported by Howald *et al.* [31]. The two independent measurements were found to be in absolute agreement within $\pm 5\%$ over the entire energy range.

E. Experimental uncertainties

A summary of the estimated experimental uncertainties in the determination of absolute cross sections with this apparatus is presented in Table I. In addition to the statistical uncertainties in the ionized ion counts, other sources of systematic uncertainties were evaluated to determine the total uncertainty in the absolute cross-section measurements. Fluctuations in the intensities of the parent beams tended to be averaged out over many scans of the electron gun across the ion beam, but still affected the accuracy of the cross sections in some cases. At low electron energy (near threshold), the cross sections are small and the spatial extent of the beam overlap region increased due to less effective focusing of the electron beam. Space-charge interaction between the primary beams also caused the background to vary with the position of the electron beam under some conditions. This effect depended on the tuning of the ion beam and the gas pressure in the chamber [29]. The relative uncertainty of the cross section at low energies in some cases significantly exceeded the statistical uncertainty determined by the ionized ion count rate. The electron-ion signal was obtained by back-

ground subtraction, where the background was determined from the ionized ion counts accumulated in the two extreme regions of the travel of the electron gun where the electron beam did not intersect the ion beam. The number of translations of the electron beam across the ion beam that were required to obtain a satisfactory cross-section measurement depended on the electron energy and the stability of the beams, and was much larger at low electron energies. Such a cross-section measurement at a given electron energy was repeated several times and the reported cross-section values represent the variance-weighted mean of those measurements.

III. EXPERIMENTAL RESULTS AND ANALYSIS

A. Excitation and ionization energies

To facilitate identification of contributions of different ionization mechanisms to the measured total ionization cross sections, the relevant subshell excitation and ionization energies were calculated using the Hartree-Fock atomic structure computer code of Cowan [32]. Table II shows the calculated ionization threshold energies in eV for removal of electrons from specific subshells of the charge states of Mn under consideration. Configuration-averaged transition energies for relevant inner-shell excitations of Mn^{5+} , Mn^{6+} , Mn^{7+} , and Mn^{8+} were also calculated, and are presented in Table III.

B. Ionization cross-section measurements

1. $\text{Mn}^{5+} \rightarrow \text{Mn}^{6+}$

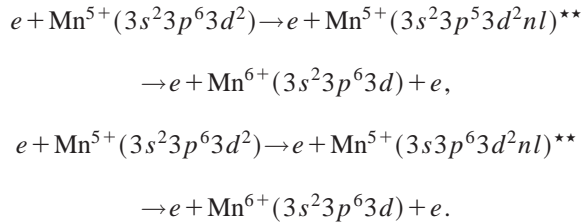
The measured absolute cross section for electron-impact single ionization of Mn^{5+} , which is a member of the Ca isoelectronic sequence, is plotted in Fig. 2 and tabulated in Table IV. The dashed curve represents a semiempirical estimate for direct ionization from the $3d$, $3p$, and $3s$ subshells using the Lotz semiempirical formula [2]. Direct ionization of the L shell has not been included since subsequent autoionization would lead to double ionization of Mn^{5+} . The cross section rises much more steeply from zero at the ionization threshold energy of 95 eV than would be expected for direct ionization. Based on the calculated transition energies presented in Table III, this enhancement is attributed to ex-

TABLE II. Calculated ionization threshold energies for different subshells of Mn^{q+} ions.

Ion	Subshell	Energy (eV)
Mn^{5+}	$3d$	95
Mn^{5+}	$3p$	145
Mn^{5+}	$3s$	185
Mn^{5+}	$2p$	753
Mn^{5+}	$2s$	874
Mn^{6+} ^a	$4s$	80
Mn^{6+}	$3d$	119
Mn^{6+}	$3p$	163
Mn^{6+}	$3s$	209
Mn^{6+}	$2p$	783
Mn^{6+}	$2s$	911
Mn^{7+}	$3p$	195
Mn^{7+}	$3s$	236
Mn^{7+}	$2p$	817
Mn^{7+}	$2s$	945
Mn^{8+} ^a	$3d$	178
Mn^{8+}	$3p$	221
Mn^{8+}	$3s$	287
Mn^{8+}	$2p$	851
Mn^{8+}	$2s$	979

^aMetastable state.

citation of the $3p$ and $3s$ subshells, followed by autoionization:



Although only configuration-averaged excitation energies are presented in Table III, it should be noted that the fine structure gives rise to large numbers of individual transitions with different excitation energies. For example, there are 90 transitions spanning an energy range of 12 eV for $3s \rightarrow 5p$ excitation of Mn^{5+} , and 386 transitions spanning 28 eV for $3p \rightarrow 5d$. The calculated energies for some of these excitations are therefore indicated by horizontal bands in Fig. 2, and only configuration-averaged transition energies are indicated on the energy-level diagram in Fig. 3. Because of the large number of possible transitions, and the fact that these channels remain open at energies above their thresholds, it is unlikely that structure due to excitation-autoionization will be evident in the total ionization cross section in this case. The lowest-energy excitation that can lead to autoionization is a $3p \rightarrow 4p$ monopole transition with a mean excitation energy of 97 eV, which is just above the Mn^{5+} ionization threshold. In this case, the calculation indicates that 58 of the 256 possible transitions between fine-structure levels lie above the ionization limit, and may therefore in principle

TABLE III. Calculated configuration-averaged inner-shell excitation energies for Mn^{q+} ions.

Ion	Transition	Energy (eV)
Mn^{5+}	$3s^23p^63d^2 \rightarrow 3s^23p^53d^24p$	97
Mn^{5+}	$3s^23p^63d^2 \rightarrow 3s^23p^53d^24d$	110
Mn^{5+}	$3s^23p^63d^2 \rightarrow 3s^23p^53d^24f$	120
Mn^{5+}	$3s^23p^63d^2 \rightarrow 3s^23p^53d^25p$	121
Mn^{5+}	$3s^23p^63d^2 \rightarrow 3s^23p^53d^25d$	128
Mn^{5+}	$3s^23p^63d^2 \rightarrow 3s3p^63d^24s$	125
Mn^{5+}	$3s^23p^63d^2 \rightarrow 3s3p^63d^24p$	126
Mn^{5+}	$3s^23p^63d^2 \rightarrow 3s3p^63d^24d$	139
Mn^{5+}	$3s^23p^63d^2 \rightarrow 3s3p^63d^25p$	155
Mn^{5+}	$3s^23p^63d^2 \rightarrow 3s3p^63d^25d$	161
Mn^{6+}	$3s^23p^63d \rightarrow 3s^23p^53d4d$	121
Mn^{6+}	$3s^23p^63d \rightarrow 3s^23p^53d5p$	136
Mn^{6+}	$3s^23p^63d \rightarrow 3s^23p^53d5d$	143
Mn^{6+}	$3s^23p^63d \rightarrow 3s3p^63d4s$	137
Mn^{6+}	$3s^23p^63d \rightarrow 3s3p^63d4p$	139
Mn^{6+}	$3s^23p^63d \rightarrow 3s3p^63d4d$	153
Mn^{6+}	$3s^23p^63d \rightarrow 3s3p^63d5s$	166
Mn^{6+}	$3s^23p^63d \rightarrow 3s3p^63d5p$	169
Mn^{7+}	$3s^23p^6 \rightarrow 3s3p^65d$	199
Mn^{7+}	$3s^23p^6 \rightarrow 3s3p^66s$	200
Mn^{7+}	$3s^23p^6 \rightarrow 3s3p^66p$	205
Mn^{7+}	$3s^23p^6 \rightarrow 3s3p^67s$	214
Mn^{7+}	$3s^23p^6 \rightarrow 3s3p^67p$	224
Mn^{7+}	$2p^63s^23p^6 \rightarrow 2p^53s^23p^63d$	658
Mn^{8+}	$3s^23p^43d \rightarrow 3s^23p^33d4d$	190
Mn^{8+}	$3s^23p^43d \rightarrow 3s3p^43d4d$	220
Mn^{8+}	$3s^23p^5 \rightarrow 3s3p^55d$	221
Mn^{8+}	$3s^23p^5 \rightarrow 3s3p^56p$	223
Mn^{8+}	$3s^23p^5 \rightarrow 3s3p^59p$	242
Mn^{8+}	$2p^63s^23p^5 \rightarrow 2p^53s^23p^53d$	662

contribute to the ionization cross section. Of course, in addition to the excitation cross section, the branching ratio for autoionization versus radiative decay of a core-excited level determines the contribution of a given excitation to the total ionization cross section.

The solid curve in Fig. 2 represents a distorted-wave theoretical calculation [33] that includes both direct ionization of the M shell, and contributions due to excitation-autoionization of $3s$ and $3p$ electrons. While the calculation agrees with the measurements within the experimental uncertainty at electron energies above 500 eV, it underestimates them by 20% at the cross-section maximum, and even more significantly at energies close to the threshold. This suggests that the calculation may be accurately accounting for the dipole-allowed excitations, but underestimating nondipole excitations such as $3p \rightarrow 4p$, for which the cross section is expected to increase steeply just above the ionization threshold, and to fall off much more rapidly with increasing electron energy E (asymptotically, $\sigma \propto 1/E$ for dipole-forbidden excitations, and $\sigma \propto \ln E/E$ for dipole-allowed excitations and for direct ionization) [34].

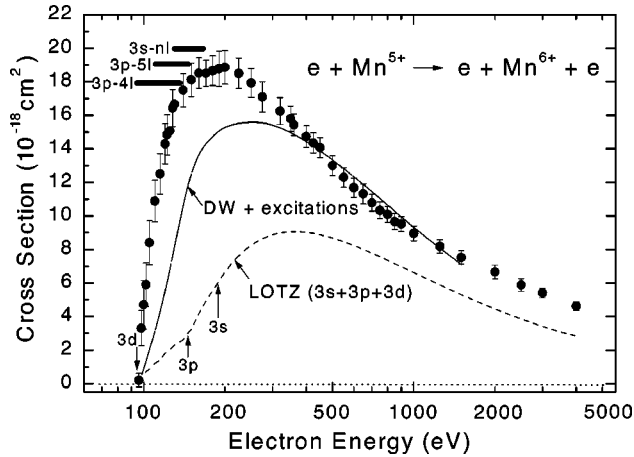


FIG. 2. Absolute single ionization cross-section measurements for Mn^{5+} as a function of electron-impact energy. The dashed curve is the sum of the predictions of the Lotz semiempirical formula for direct ionization of $3s$, $3p$, and $3d$ electrons, whose threshold energies are indicated by vertical arrows. The solid curve is a distorted-wave theoretical calculation [33] that includes contributions from both direct ionization and $3l \rightarrow n'l'$ excitation-autoionization. The ranges of thresholds for some possible inner-shell excitation-autoionization transitions are indicated by horizontal energy bands.

2. $\text{Mn}^{6+} \rightarrow \text{Mn}^{7+}$

Absolute cross-section measurements for electron-impact single ionization of Mn^{6+} are compared to predictions of the Lotz formula for direct ionization in Fig. 4 and tabulated in Table IV. A member of the K isoelectronic sequence, the ground-state configuration of Mn^{6+} is $3s^2 3p^6 3d$, which has an ionization threshold energy of 119 eV. The rise in the experimental cross-section at electron energies below 119 eV is attributed to a $\text{Mn}^{6+} 3s^2 3p^6 4s$ metastable component in the primary ion beam from the ECR ion source, for which the ionization threshold is 80 eV. The maximum ionization cross section for Mn^{6+} is only 15% smaller than that for Mn^{5+} , and the ionization cross section for Mn^{6+} similarly exhibits a strong onset just above the single ionization threshold from the ground state at 119 eV. This steep rise is attributed at least in part to $3p \rightarrow 4d$ inner-shell excitation, followed by autoionization, which again occurs just above the ground-state ionization threshold and appears to dominate the total ionization cross section. Excitations of $3p$ electrons to higher levels, as well as $3s$ excitation, likely also contribute to the single ionization cross section, but analysis is less straightforward than for Mn^{5+} because of an undetermined population of the $\text{Mn}^{6+} 4s$ metastable state in the reactant beam. A theoretical calculation in progress for Mn^{6+} [35] based on the binary-encounter-Bethe method that includes both direct ionization and some dipole-allowed excitation-autoionization contributions lies significantly below the measurements, and suggests a large metastable component in the experiment.

Large indirect ionization contributions were found for Ti^{3+} , which is isoelectronic with Mn^{6+} , and for which $3p \rightarrow 3d$ excitation-autoionization dominates the single ionization cross section just above the ionization threshold energy

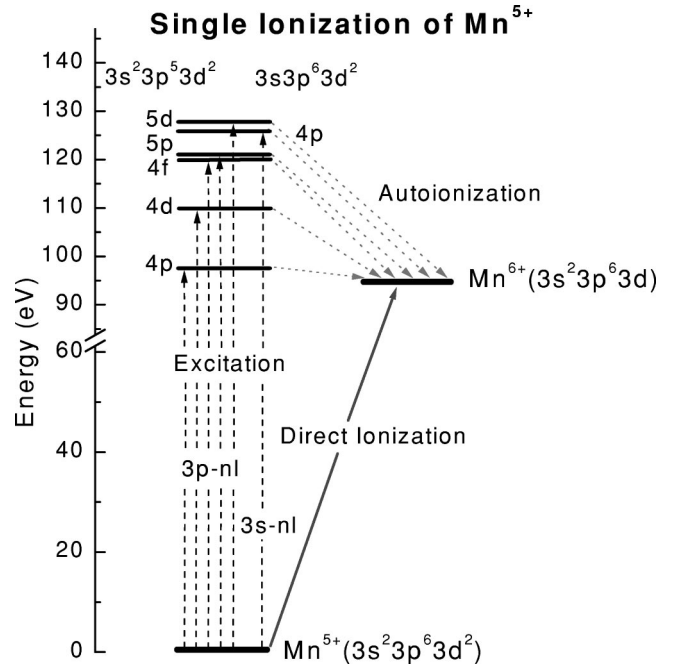
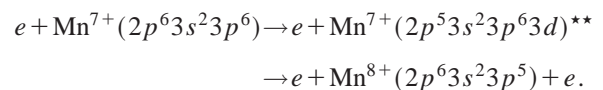


FIG. 3. Energy-level diagram showing direct and some excitation-autoionization pathways for single ionization from the ground state of Mn^{5+} . For clarity, only the average energy for each core-excited configuration is indicated.

by more than an order of magnitude [6,7]. For Mn^{6+} , however, excitation-autoionization due to $\Delta n = 0$ transitions is not possible energetically.

3. $\text{Mn}^{7+} \rightarrow \text{Mn}^{8+}$

Absolute cross-section measurements for electron-impact single ionization of Mn^{7+} are compared to predictions of the Lotz formula for direct ionization in Fig. 5 and tabulated in Table IV. Mn^{7+} is Ar-like, with a $3s^2 3p^6$ closed-subshell ground-state configuration and an ionization potential of 195 eV. The $3s$ and $3p$ electrons are more tightly bound than in Mn^{5+} and Mn^{6+} , resulting in a smaller ionization cross section. Though the maximum ionization cross section for Mn^{7+} is only 30% of that for Mn^{6+} , the relative contribution of indirect to direct ionization is estimated to be comparable at the peaks in the respective cross sections. The excitations that are expected to lead to autoionization in this case are $3s \rightarrow nl$ with $n \geq 5$. The cross section exhibits a broad maximum at energies above 325 eV, suggesting an increased relative role of dipole-allowed excitations. The apparent enhancement of the cross section at higher energy may be attributable to an increased relative role of L -shell excitation followed by autoionization:



4. $\text{Mn}^{8+} \rightarrow \text{Mn}^{9+}$

Absolute cross-section measurements for electron-impact single ionization of Mn^{8+} are compared to predictions of the

TABLE IV. Measured absolute electron-impact single ionization cross sections and total uncertainties for Mn^{q+} ions.

Mn^{5+}		Mn^{6+}		Mn^{7+}		Mn^{8+}	
E (eV)	σ (10^{-18} cm 2)	E (eV)	σ (10^{-18} cm 2)	E (eV)	σ (10^{-18} cm 2)	E (eV)	σ (10^{-18} cm 2)
96	0.22 ± 0.34	82	-0.10 ± 1.00	190	-0.10 ± 0.40	178	-0.03 ± 0.05
98	3.30 ± 1.05	92	0.60 ± 0.65	200	0.87 ± 0.50	180	0.05 ± 0.05
100	4.71 ± 1.45	101	1.10 ± 0.60	210	1.87 ± 0.35	200	0.12 ± 0.10
102	5.92 ± 1.30	113	1.20 ± 0.80	212	2.88 ± 0.36	210	0.21 ± 0.14
105	8.43 ± 1.30	118	3.80 ± 1.10	216	3.16 ± 0.33	220	0.62 ± 0.20
110	10.88 ± 1.25	123	6.34 ± 0.95	220	3.67 ± 0.30	230	0.92 ± 0.20
115	12.51 ± 1.20	128	7.85 ± 0.92	230	4.12 ± 0.33	235	1.16 ± 0.25
120	14.33 ± 1.20	132	9.55 ± 0.93	240	4.36 ± 0.35	240	1.46 ± 0.18
122	14.84 ± 1.20	140	11.24 ± 0.90	250	4.56 ± 0.36	245	1.63 ± 0.16
125	15.06 ± 1.21	144	12.80 ± 1.02	275	4.68 ± 0.37	250	1.92 ± 0.15
128	16.43 ± 1.31	153	13.46 ± 1.08	300	4.91 ± 0.39	260	2.25 ± 0.18
130	16.66 ± 1.33	162	13.86 ± 1.11	325	5.01 ± 0.40	275	2.48 ± 0.20
140	17.50 ± 1.40	173	14.77 ± 1.18	350	5.08 ± 0.41	300	2.63 ± 0.21
150	18.12 ± 1.45	185	13.38 ± 1.07	375	5.11 ± 0.41	325	2.74 ± 0.22
160	18.52 ± 1.45	194	15.55 ± 1.24	400	5.10 ± 0.41	350	2.78 ± 0.22
170	18.51 ± 1.45	205	15.56 ± 1.24	425	5.08 ± 0.41	375	2.87 ± 0.23
180	18.66 ± 1.49	214	15.84 ± 1.27	450	5.07 ± 0.41	400	2.92 ± 0.23
190	18.78 ± 1.50	228	15.80 ± 1.26	500	5.07 ± 0.41	450	2.97 ± 0.24
200	18.86 ± 1.51	234	15.69 ± 1.26	525	5.05 ± 0.40	500	2.99 ± 0.24
225	18.50 ± 1.48	250	15.52 ± 1.24	550	5.01 ± 0.40	550	2.97 ± 0.24
250	17.93 ± 1.43	270	15.41 ± 1.23	575	5.01 ± 0.40	600	2.98 ± 0.24
275	17.10 ± 1.37	290	14.92 ± 1.19	600	4.98 ± 0.40	700	2.98 ± 0.24
320	16.25 ± 1.30	310	14.25 ± 1.14	650	4.88 ± 0.39	800	2.92 ± 0.23
360	15.43 ± 1.23	348	13.49 ± 1.08	700	4.75 ± 0.38	850	2.88 ± 0.23
400	14.73 ± 1.18	374	13.03 ± 1.04	750	4.63 ± 0.37	900	2.87 ± 0.23
500	13.00 ± 1.04	400	12.80 ± 1.02	800	4.48 ± 0.36	1000	2.72 ± 0.22
550	12.30 ± 0.98	434	12.23 ± 0.98	850	4.36 ± 0.35	1250	2.46 ± 0.20
600	11.68 ± 0.93	526	10.92 ± 0.87	900	4.27 ± 0.34	1500	2.29 ± 0.18
650	11.31 ± 0.90	578	10.43 ± 0.83	1000	4.08 ± 0.33	2000	2.08 ± 0.17
700	10.78 ± 0.86	631	9.90 ± 0.79	1250	3.70 ± 0.30	2500	1.82 ± 0.15
750	10.33 ± 0.83	675	9.70 ± 0.78	1500	3.42 ± 0.27	3000	1.59 ± 0.13
800	10.08 ± 0.81	745	9.16 ± 0.73	2000	2.88 ± 0.23	4000	1.34 ± 0.11
900	9.51 ± 0.76	800	8.88 ± 0.71	2500	2.53 ± 0.20		
1000	8.96 ± 0.72	850	8.51 ± 0.68	3000	2.20 ± 0.18		
1250	8.18 ± 0.65	900	8.23 ± 0.66	4000	1.88 ± 0.15		
1500	7.52 ± 0.60	1000	7.75 ± 0.62				
2000	6.66 ± 0.53	1201	7.21 ± 0.58				
2500	5.88 ± 0.47	1503	6.42 ± 0.51				
3000	5.40 ± 0.43	2007	5.54 ± 0.44				
4000	4.62 ± 0.37	3009	4.28 ± 0.34				
		4012	3.52 ± 0.10				

Lotz formula for direct ionization in Fig. 6 and are tabulated in Table IV. The peak ionization cross section for Mn^{8+} is approximately 60% of that for Mn^{7+} , and the onset of ionization is observed at approximately 178 eV, significantly below the threshold for removal of the outer $3p$ electron at 221 eV. This indicates that the primary Mn^{8+} ion beam contains a significant population in the $3s^23p^43d$ metastable state that lies 43 eV above the $3s^23p^5$ ground state, as was found in similar measurements for other members of the Cl

isoelectronic sequence: Ti^{5+} [9], Cr^{7+} [12], and Fe^{9+} [13]. The energy-level calculations indicate that the lowest-energy excitations that can lead to autoionization in the case of Mn^{8+} are $3s \rightarrow 5p$ (for the ground state) and $3p \rightarrow 4d$ (for the metastable component). Using the Lotz formula as an estimate for the direct ionization cross section, the ratio of the peak cross section to that for direct ionization is estimated to be approximately 1.4. As for Mn^{7+} , the cross section may also be enhanced at higher incident energies by a

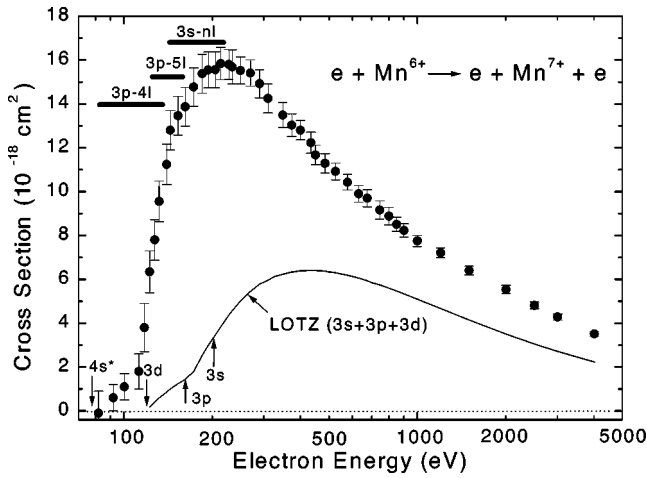


FIG. 4. Absolute single ionization cross-section measurements for Mn^{6+} as a function of electron-impact energy. The solid curve is the sum of the predictions of the Lotz semiempirical formula for direct ionization of $3s$, $3p$, and $3d$ electrons from the $3p^6 3d$ ground state, whose thresholds are indicated by vertical arrows. The ionization threshold from the $3p^6 4s$ metastable state at 80 eV is also indicated as $4s^*$. The range of thresholds for some possible inner-shell excitation-autoionization contributions are indicated by horizontal energy bands.

contribution from excitation of an L -shell electron followed by autoionization, contributing to the broad maximum in the total ionization cross section.

C. Systematics along isoelectronic sequences

To investigate possible systematic effects related to the relative role of indirect versus direct ionization, it is instructive to compare total ionization cross-section measurements with predictions for direct outer-shell ionization. Table V

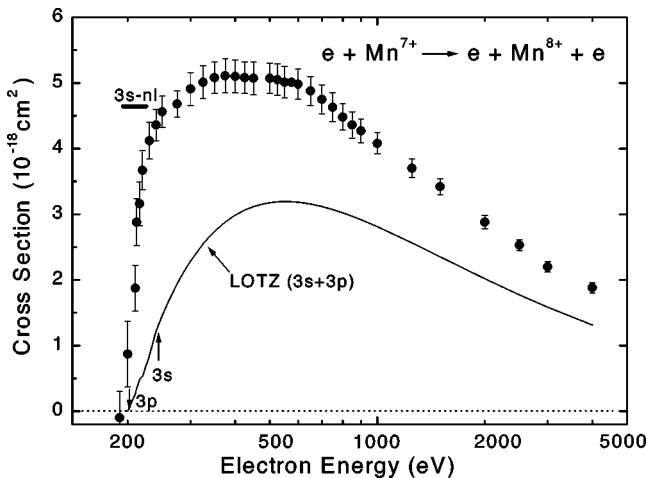


FIG. 5. Absolute single ionization cross-section measurements for Mn^{7+} as a function of electron-impact energy. The solid curve is the sum of the predictions of the Lotz semiempirical formula for direct ionization of $3s$ and $3p$ electrons, whose thresholds are indicated by vertical arrows. Thresholds for some possible inner-shell excitation-autoionization contributions are indicated by horizontal energy bands.

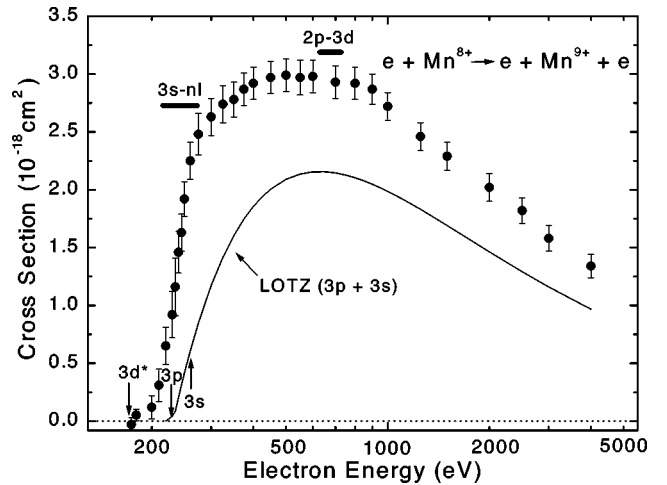


FIG. 6. Absolute single ionization cross-section measurements for Mn^{8+} as a function of electron-impact energy. The solid curve is the sum of the predictions of the Lotz semiempirical formula for direct ionization of $3s$ and $3p$ electrons from the $3s^2 3p^5$ ground state, whose thresholds are indicated by vertical arrows. The threshold for direct ionization from the metastable $3s^2 3p^4 3d$ level at 178 eV is also indicated as $3d^*$. Thresholds for some possible inner-shell excitation-autoionization contributions from the ground state are indicated by horizontal energy bands.

presents a comparison of measured peak ionization cross sections to the maximum value for direct ionization predicted by the Lotz formula for metallic ions of the Ca, K, Ar, and Cl isoelectronic sequences. For the Ar and Cl isoelectronic sequences, the ratio of indirect to direct ionization increases monotonically with nuclear charge Z . This ratio is largest and approximately constant for the K sequence, and decreases monotonically with Z for the Ca sequence. The present measurements are consistent with published experimental data for isoelectronic multiply charged metal ions, and emphasize the important contributions of indirect ionization.

IV. SUMMARY

Absolute cross-section measurements using a new dynamic-crossed-beams apparatus are reported. The measure-

TABLE V. Ratios of measured peak ionization cross sections to the maximum value for direct ionization predicted by the Lotz formula for the Ca, K, Ar, and Cl isoelectronic sequences.

Element	Z	Ca sequence	K sequence	Ar sequence	Cl sequence
Ti	22	2.3 ^a	2.6 ^b		1.1 ^c
Cr	24			1.4 ^d	1.2 ^d
Mn	25	2.1	2.5	1.6	1.4
Fe	26	1.8 ^e			1.5 ^e
Ni	28	1.6 ^f			

^aReference [8].

^bReference [7].

^cReference [9].

^dReference [12].

^eReference [13].

^fReference [19].

ments for electron-impact single ionization of Mn^{q+} ($5 \leq q \leq 8$) are systematically consistent with published experimental data for isoelectronic multiply charged ions of Ti, Cr, Fe, and Ni, and emphasize the importance of inner-shell excitation-autoionization for these metallic ions. The relative enhancement of the total ionization cross sections is largest at energies just above the ionization threshold, and therefore is expected to significantly affect the ionization balance in plasma environments where such ions exist. Comparison of experiment and theory for Mn^{5+} suggests that dipole-forbidden inner-shell excitations may be contributing more significantly than predicted by a distorted-wave calculation in the threshold energy region. Agreement between theory and experiment at energies well above the cross-section maximum suggests that the theory includes and accurately accounts for both direct ionization and the dominant dipole-allowed indirect ionization channels. Further development of the crossed-beams apparatus is underway to permit measurement of the energies of ejected electrons from such collisions. This will facilitate more direct identification and quan-

tification of the role of the various indirect ionization channels.

ACKNOWLEDGMENTS

The authors are most grateful to E. Salzbom for contributing the electron gun used for these measurements, and to R. E. H. Clark and Y.-K. Kim for communicating the results of unpublished theoretical calculations. The assistance of R. Mancini and H. Merabet with implementation of the Cowan atomic-structure code is gratefully acknowledged. Special thanks are also due to J. K. Swenson and P. Bible for contributions to the design and modeling of the crossed-beam apparatus, to W. Cline, D. Meredith, and W. Weaver for their expertise in its mechanical design and fabrication, and to W. Brinsmead for resourcefulness in acquiring several critical components. This research was supported by the Division of Chemical Sciences, Office of Basic Energy Sciences of the U.S. Department of Energy under Contract No. DE-FG03-97ER14787, and by the Nevada DOE/EPSCoR program in Chemical Physics.

-
- [1] F. Brouillard and J. W. McGowan, *Physics of Ion-Ion and Electron-Ion Collisions* (Plenum, New York, 1983). For applications in astrophysics and fusion energy, see articles by A. Dalgarno, p. 1, and D. E. Post, p. 37, respectively.
- [2] W. Lotz, *Z. Phys.* **216**, 241 (1968); **220**, 466 (1969).
- [3] G. H. Dunn, in *Electron-Impact Ionization*, edited by T. D. Märk and G. H. Dunn (Springer-Verlag, New York, 1985), pp. 277–319.
- [4] A. Müller, in *Physics of Ion Impact Phenomena*, edited by D. Mathur (Springer-Verlag, Berlin, 1991), pp. 13–90.
- [5] M.S. Pindzola, T.W. Gorczyca, N.R. Badnell, D.C. Griffin, M. Stenke, G. Hofmann, B. Weissbecker, K. Tinschert, E. Salzbom, A. Müller, and G.H. Dunn, *Phys. Rev. A* **49**, 933 (1994).
- [6] R.A. Falk, G.H. Dunn, D.C. Griffin, C. Bottcher, D.C. Gregory, D.H. Crandall, and M.S. Pindzola, *Phys. Rev. Lett.* **47**, 494 (1981).
- [7] R.A. Falk, G.H. Dunn, D.C. Gregory, and D.H. Crandall, *Phys. Rev. A* **27**, 762 (1983).
- [8] D.W. Mueller, T.J. Morgan, G.H. Dunn, D.C. Gregory, and D.H. Crandall, *Phys. Rev. A* **31**, 2905 (1985).
- [9] S.J. Chantrenne, D.C. Gregory, M.J. Buie, M.S. Pindzola, *Phys. Rev. A* **41**, 140 (1990).
- [10] U. Hartenfeller, K. Aichele, D. Hathiramani, G. Hofmann, V. Schäffer, M. Steidl, M. Stenke, E. Salzbom, and M.S. Pindzola, *J. Phys. B* **31**, 2999 (1998).
- [11] U. Hartenfeller, K. Aichele, D. Hathiramani, V. Schäfer, M. Steidl, F. Scheuermann, and E. Salzbom, *J. Phys. B* **31**, 3013 (1998).
- [12] M. Sataka, S. Ohtani, D. Swenson, and D.C. Gregory, *Phys. Rev. A* **39**, 2397 (1989).
- [13] D.C. Gregory, F.W. Meyer, A. Müller, and P. Defrance, *Phys. Rev. A* **34**, 3657 (1986).
- [14] D.C. Gregory, L.J. Wang, F.W. Meyer, and K. Rinn, *Phys. Rev. A* **35**, 3256 (1987).
- [15] M. Stenke, K. Aichele, U. Hartenfeller, D. Hathiramani, M. Steidl, and E. Salzbom, *J. Phys. B* **32**, 3627 (1999).
- [16] M. Stenke, U. Hartenfeller, K. Aichele, D. Hathiramani, M. Steidl, and E. Salzbom, *J. Phys. B* **32**, 3641 (1999).
- [17] D.C. Gregory and A.M. Howald, *Phys. Rev. A* **34**, 97 (1986).
- [18] M. Stenke, D. Hathiramani, G. Hofmann, V.P. Shevelko, M. Steidl, R. Volpel, and E. Salzbom, *Nucl. Instrum. Methods Phys. Res. B* **98**, 138 (1995).
- [19] L.J. Wang, K. Rinn, and D.C. Gregory, *J. Phys. B* **21**, 2117 (1988).
- [20] D.C. Griffin, C. Bottcher, and M.S. Pindzola, *Phys. Rev. A* **25**, 1374 (1982).
- [21] M.S. Pindzola, D.C. Griffin, and C. Bottcher, *Phys. Rev. A* **34**, 3668 (1986).
- [22] D.C. Griffin and M.S. Pindzola, *J. Phys. B* **21**, 3253 (1988).
- [23] F. Brouillard and P. Defrance, *Phys. Scr.* **3**, 801 (1983).
- [24] A. Müller, K. Huber, K. Tinschert, R. Becker, and E. Salzbom, *J. Phys. B* **18**, 2993 (1985).
- [25] R.A. Phaneuf *et al.*, in *Applications of Accelerators in Research and Industry: Proceedings of the Fourteenth International Conference*, AIP Conf. Proc. No. 392 (AIP, Woodbury, NY, 1997).
- [26] D. Hitz, P. Ludwig, G. Melin, and M. Pontonnier, *Nucl. Instrum. Methods Phys. Res. B* **98**, 517 (1995).
- [27] M. Stenke, K. Aichele, D. Hathiramani, G. Hofmann, M. Steidl, R. Volpel, and E. Salzbom, *Nucl. Instrum. Methods Phys. Res. B* **98**, 573 (1995).
- [28] G. Hofmann, A. Müller, K. Tinschert, and E. Salzbom, *Z. Phys. C* **16**, 113 (1990).
- [29] A. Müller, G. Hofmann, K. Tinschert, R. Sauer, and E. Salzbom, *Nucl. Instrum. Methods Phys. Res. B* **24/25**, 369 (1987).
- [30] K. Rinn, A. Müller, H. Eichenauer, and E. Salzbom, *Rev. Sci. Instrum.* **53**, 829 (1982).

- [31] A.M. Howald, D.C. Gregory, F.W. Meyer, R.A. Phaneuf, A. Müller, N. Djuric, and G.H. Dunn, *Phys. Rev. A* **33**, 3779 (1986).
- [32] R. D. Cowan, *The Theory of Atomic Structure and Spectra* (University of California Press, Berkeley, 1981).
- [33] R. E. H. Clark (private communication); R. Rejoub, R. E. H. Clark, and R. A. Phaneuf, in *Proceedings of the XXI International Conference on the Physics of Electronic and Atomic Collisions, Sendai, Japan, 1999* (The University of Electro-Communications, Tokyo, 1999), p. 359.
- [34] R. A. Phaneuf, in *Atomic Processes in Electron-Ion and Ion-Ion Collisions*, edited by F. Brouillard (Plenum, New York, 1986), p. 119.
- [35] K. Moribayashi and Y.-K. Kim, in *Proceedings of the XXI International Conference on the Physics of Electronic and Atomic Collisions, Sendai, Japan, 1999* (Ref. [33]), p. 363.